Express Polymer Letters Vol.18, No.7 (2024) 675–688
Available online at www.expresspolymlett.com
https://doi.org/10.3144/expresspolymlett.2024.50

Research article

Construction and applications of superhydrophilic surface based on ethylene-vinyl acetate copolymer/nitrile-butadiene rubber thermoplastic vulcanizate

*Weiran Zhang, Yuan Gao, Ruotao Feng, Dazhi Zhu, Zhaobo Wang**

College of Materials Science & Engineering, Qingdao University of Science & Technology, 266042 Qingdao, P. R. China

Received 6 March 2024; accepted in revised form 18 April 2024

Abstract. In this research, a straightforward template method was utilized to fabricate a superhydrophilic ethylene-vinyl acetate copolymer (EVA)/nitrile-butadiene rubber (NBR) thermoplastic vulcanizate (TPV) surface where the paper sheet was used as template. Organic modified montmorillonite (OMMT) powder was introduced in order to improve the superhydrophilic response rate of the TPV surface. Investigations were conducted to research the durability and the self-cleaning behavior of the TPV surface, as well as to explore its potential application in the separation of oil-water and oil-oil mixtures. Experimental results demonstrated that the EVA/NBR/OMMT TPV (mass ratio 20/80/7) surface molded with No. 1000 paper sheet exhibited the excellent superhydrophilic property, which could achieve a contact angle of 0.0° within 5.5 s and had a surface energy of 35.6 $mN \cdot m^{-1}$. The superhydrophilic surface displayed the remarkable durability and the evident self-cleaning behavior; moreover, it could exhibit the significant difference in the critical pressure data for various liquids, suggesting the promising application in the field of oil-water and oil-oil separation.

Keywords: *thermoplastic elastomer, surface modification, surface property, functional polymer, hydrophilicity, superhydrophilic*

1. Introduction

Thermoplastic vulcanizate (TPV) is produced by incorporating rubber pre-blend into thermoplastic resin through dynamic vulcanization, usually resulting in a two-phase microstructure where the resin phase and the rubber phase is the continuous phase and the dispersed phase, respectively [1, 2]. The microstructure enables the TPV to exhibit the plasticity behavior at the elevated temperatures while maintaining the thermoplastic property at room temperature. The TPV offers the advantages such as low production cost, straightforward manufacturing process and simple equipment; moreover, the resulting product can be tailored for a wide range of characteristics [3]. The wettability of the solid surface plays a crucial role in both theoretical and application [4]. In the recent years, the research on the superhydrophilic surface and superhydrophobic surface of solid materials has obtained the significant attention [5]. Regulating the contact angle of the material surface or adjusting the difference between the surface energy (SFE) of the material surface and the surface tension of the liquid can effectively achieve the desired wettability [6]. The characteristic of superhydrophobicity is that water does not adhere to the surface [7]. By studying and imitating the superhydrophobic phenomenon in nature, people have developed biomimetic superhydrophobic materials with the advantages such as self-cleaning [8], oil repellency [9] and low adhesion [10], which have broad application prospects in petrochemicals [11], environmental protection [12], biomedicine [13] and other fields. The common methods for preparing superhydrophobic surfaces include increasing surface roughness and reducing

*Corresponding author, e-mail: wangzhb.cn@gmail.com

SFE, such as electrospinning [14], electrochemical methods [15] and layer-by-layer methods [16]. The characteristic of superhydrophilicity is that water spreads completely on the surface [7]. Generally, superhydrophilic materials are defined as the materials with the solid-liquid contact angles less than 10.0° or close to 0.0° [17]. In 1997, Wang *et al*. [18] firstly reported the superhydrophilic surface of titanium dioxide with the contact angle approaching 0.0°. Due to their unique wetting properties, the superhydrophilic surfaces offer the distinct advantages, including self-cleaning [19, 20], anti-fogging [20] and efficient heat conduction [21]. These properties have the significant applications in the areas such as antifouling, anti-fogging and oil-water separation [22, 23]. Currently, several methods for preparing superhydrophilic surfaces have been reported, including sol-gel method [24], vapor deposition [25], templating [26], phase separation [27] and layer-by-layer self-assembly [28]. Among these methods, the template method is the highly favored for its simplicity, high efficiency, scalability, cost-effectiveness and practicality [29].

Superhydrophilic surface technology, as a branch of biomimetic nanomaterials technology, has made the significant progress in both the theoretical research and the practical application [30]. However, there has been relatively little research on the polymer-based superhydrophilic materials. Polymer-based materials typically exhibit the surface inertness and the hydrophobicity, making it challenging to achieve the superhydrophilic modification. Literatures on the superhydrophilic modification based on the polymer matrix surfaces primarily employ several main methods, including plasma treatment [31], nanocoating [32], surface grafting modification [33], physical surface roughening and diverse modification approaches. Classic wetting theories propose that constructing a superhydrophilic surface comprises two essential aspects: creating surface rough structures and modifying the hydrophilic functional groups. The key to constructing a superhydrophilic surface lies in building the rough surface microstructure.

Tsougeni *et al*. [34] achieved the superhydrophilicity by employing anisotropic oxygen plasma etching on the surfaces of poly(methyl methacrylate) and poly (ether ether ketone). However, the plasma treatment method leads to the high costs and the durability of the treated surface is generally moderate. Zheng *et al*. [35] embedded $CaCO_3$ nanoparticles into the surface of low-density polyethylene using a hot-pressing technique and created a polymer based superhydrophilic surface. However, its superhydrophilic properties have not been thoroughly explored, lacking further research results. Usha *et al*. [36] transformed the biaxially hydrophobic polypropylene film into a permanent superhydrophilic film with underwater superoleophobic using corona discharge treatment and grafting method. This superhydrophilic film can be used for gravity separation. However, the grafting method is time-consuming and expensive, making it unsuitable for large-scale industrial production applications. Chen *et al*. [37] prepared an underwater superoleophobic/superhydrophilic film with oil-water separation and self-cleaning properties by electrochemically oxidizing lignin sulfonate-doped polypyrrole. However, the limitations of electrode materials have long restricted the use of the electrochemical method in industrial applications due to its low current efficiency and high energy consumption, particularly in the challenging degradation of organic compounds.

Ethylene-vinyl acetate copolymer (EVA) is a thermoplastic polymer composed of polar vinyl acetate and non-polar ethylene units. Compared to the most thermoplastic materials, EVA offers the several advantages, including excellent biocompatibility, good melt processability, outstanding oil resistance, low-temperature flexibility and high polarity [38, 39]. Nitrile-butadiene rubber (NBR) is a polar rubber synthesized from butadiene and acrylonitrile monmers, renowned for its excellent oil resistance, heat resistance and adhesive properties. It has the extensive applications in automotive, aerospace, petroleum and photocopying [40, 41]. In general, materials with higher polarity exhibit the better hydrophilicity; and there is potential to create the superhydrophilic surface based on the EVA/NBR TPV. Currently, there have been no discoveries of superhydrophilic polymer materials based on TPV. Many superhydrophilic materials are characterized by complex preparation methods and high production costs, making them unsuitable for large-scale industrial production. Consequently, there is an urgent need for a new type of superhydrophilic material that can be economically and produced efficiently.

In this research, EVA/NBR TPV was utilized as the matrix material while the various types of sheet papers were used as the templates. A compression molding method was employed to create the rough

microstructure in the EVA/NBR TPV surface. The research aimed to verify the feasibility of constructing superhydrophilic surfaces in the TPV surface and explored the potential applications for the prepared superhydrophilic TPV surface.

2. Experimental

2.1. Materials

EVA (3135SB), vinyl acetate mass fraction 12%, a product of DuPont Co., Ltd., Wilmington, United States. NBR (N41), combined with 29% mass fraction of acrylonitrile, a product of PetroChina Lanzhou Petrochemical Co., Ltd., Lanzhou, China.

Bis(1-(tert-butylperoxy)-1-methylethyl)-benzene (BIPB), triallyl isocyanurate (TAIC), *N*-phenyl-2-naphthylamine (antioxidant D), organic modified montmorillonite (OMMT) and other agents are all commonly used industrial grade commercially available products. TAIC comprises 30% by mass of white carbon black and 70% by mass of triallyl isocyanurate. "Xili" brand water/dry paper sheets (No. 400, No. 1000 and No. 1500), abrasive particle (aluminum oxide, Al_2O_3) size is 37, 15 and 10 μm, respectively, a product of Hubei Yuli Abrasive Belts Group Co., Ltd., Xianning, China. Cyclohexane (AR), a product of Tianjin Fuyu Fine Chemical Co., Ltd., Tianjin, China. Dodecane (AR), a product of Tianjin Kermel Analytical Reagent Co., Ltd., Tianjin, China. Ethylene glycol (AR), a product of Yantai Sanhe Chemical Reagent Co., Ltd., Yantai, China.

2.2. Specimen preparation

The peroxide crosslinked system is utilized in the NBR crosslinking formulation, which consists of the following constituents: 100 phr (per hundred rubber weight, the same as below) NBR, 3.0 TAIC, 1.3 BIPB and 1.0 antioxidant D.

In order to prepare the EVA/NBR TPV, firstly, the NBR and compounding agent were mixed in an open double roll mill (X [S] K-160, Qun Yi Rubber Machinery Co., Ltd., Shanghai, China) at room temperature to obtain NBR pre-blend. EVA particles were then melted and plasticized on an open double roll mill (SY-6215-AL1, Shi Yan Precision Instrument Co., Ltd., Dongguan China) at 165 °C and NBR preblend was put into for 8 min to obtain the dynamically vulcanized EVA/NBR compound. The rotor speed of the mixer was maintained at 43 rpm, while the EVA/NBR TPV mass ratio was fixed at 20/80. The cooled EVA/NBR compound was placed in a mold, preheated for 6 min on a plate vulcanizing machine (50 T, Qun Yi Rubber Machinery Co. Ltd., Shanghai, China) at 165 °C, exhausted for 3 times, hot pressed for 8 min and cold pressed for 8 min at a pressure of 10 MPa to obtain EVA/NBR TPV specimen.

The EVA/NBR TPV specimen was placed on the paper sheet and preheated for 10 min at 165 °C by a plate vulcanizing machine (HY4016M, Anhui Huabiao Instrument Co., Ltd., Hefei, China). After preheating, it was hot-pressed at 165 °C and 3 MPa for 3 min. Subsequently, it was transferred to another flat vulcanizing machine and cold-pressed at room temperature for 5 min at a pressure of 2 MPa. The rough surface of the EVA/NBR TPV was obtained after removing the paper sheet.

2.3. Characterization

2.3.1. Fourier transform infrared spectroscopy (FT-IR) analysis

FT-IR (TENSOR II, Bruker Daltonics GmbH & CO. KG, Bremen, Germany) was used for infrared testing of the specimens, with a scanning range of 400–4000 cm^{-1} and a resolution of 4 cm^{-1}. The OMMT powder was uniformly ground with KBr for testing in transmission reflectance (TR) mode. Solid specimens were made into 2 mm films and tested in attenuated total reflectance (ATR) mode.

2.3.2. Mechanical properties

The stress-strain behaviors of dumbbell-shaped EVA/NBR TPV at room temperature was determined on a universal material testing machine (TCS-2000, GoTech Testing Machines Inc., Taiwan, China) under a crosshead speed of 500 mm/min.

2.3.3. Static contact angle analysis

The contact angle between the rough surface of EVA/NBR TPV and deionized water was measured using a surface analyzer (LSA100, LAUDA Scientific, Lauda-Königshofen, Germany). Five different points were selected on each specimen and a microsyringe was used to dispense 5.0 μL of deionized water onto a single point of the specimen for testing.

2.3.4. SFE analysis

A surface analysis instrument was used to measure the static contact angles between a series of prepared rough surfaces of EVA/NBR TPV and deionized water, ethylene glycol and dodecane. Five points on

each specimen were selected and 5.0 μL of liquid was dispensed onto a single point using a microsyringe for testing. The SFE of each specimen was obtained by the surface analyzer in "Direct Input Mode".

2.3.5. Microscopic morphology analysis

Under the vacuum condition, a layer of platinum was sprayed onto the surface of the EVA/NBR TPV. The surface microstructure was then observed using a field emission scanning electron microscope (FE-SEM, JSM-6700F, JEOL Co., Ltd., Tokyo, Japan).

2.3.6. Self-cleaning behavior test

The dust particles were remained on the specimen surface for 30 min. Subsequently, the surface was cleaned using blowing air, water droplets and oil droplets, respectively.

2.3.7. Critical pressure test

Critical pressure (P_m) testing used for the exploration of oil-water and oil-oil separation were conducted using a self-designed separation apparatus [42]. Pm represents the external pressure value of the liquid that can flow accurately into the flask. A particular length of TPV film was wound to form a columnar structure and the required length of the TPV film was calculated according to Equation (1):

$$L = \frac{\left[\left(\frac{D}{2}\right)^2 - \left(\frac{d}{2}\right)^2\right]\pi}{h_1 + h} \quad (1)$$

where L represents the required length of the TPV film; D stands for the inner diameter of the direct suction pressure-responsive valve; d denotes the diameter of the base column of the direct suction pressure-responsive valve; h_1 signifies the thickness of the molded TPV film; h indicates the gap between wound TPV films.

In this research, the direct suction pressure-responsive valve had an inner diameter of 13 mm. The TPV film measured 700 μm in thickness and 22 mm in width. The TPV film, measuring 190 mm in length, was wound into a cylinder and cautiously inserted into the valve while ensuring a controlled film gap of 50 μm for the liquid flow.

3. Results and discussion

3.1. FT-IR analysis of OMMT, EVA and NBR vulcanizates

Figure 1 shows the FT-IR spectra of OMMT, EVA and NBR vulcanizates. Figure 1 reveals that in the spectrum of OMMT, a bending vibration absorption peak corresponding to the Si–O–Si bond is observed at 453 cm^{-1}, while absorption vibration peaks associated with the Si–O bond of OMMT are observed at 1027 and 1120 cm^{-1}, respectively. The characteristic absorption peaks of C–H symmetric and asymmetric stretching vibrations are observed at 2848 and 2921 cm^{-1}, indicating the presence of C–H bonds in the interlayer of OMMT after organic modification, with the insertion of organic carbon chains. There is also a band at 1612 and 1639 cm^{-1}, which can be attributed to the vibration absorption peak of the ammonium salt. The hydroxyl stretching vibration peak is observed at 3449 cm^{-1}.

In the infrared spectrum of NBR, the characteristic absorption peaks of the 1,2-vinyl double bond in the butadiene unit and the 1,4-double bond are observed at 914 and 966 cm^{-1}, respectively. The characteristic peak of $–CH_2$ is observed at 1455 cm^{-1}. Moreover, the stretching vibration peaks of the C–H bond in groups such as methyl and methylene are observed at 2837 and 2917 cm^{-1}. Notably, the spectrum features a stretching vibration absorption peak at 2240 cm^{-1}, which corresponds to the –CN group in the NBR.

The infrared spectrum of NBR/6.25OMMT (mass ratio 100/6.25) vulcanizate shows absorption peaks

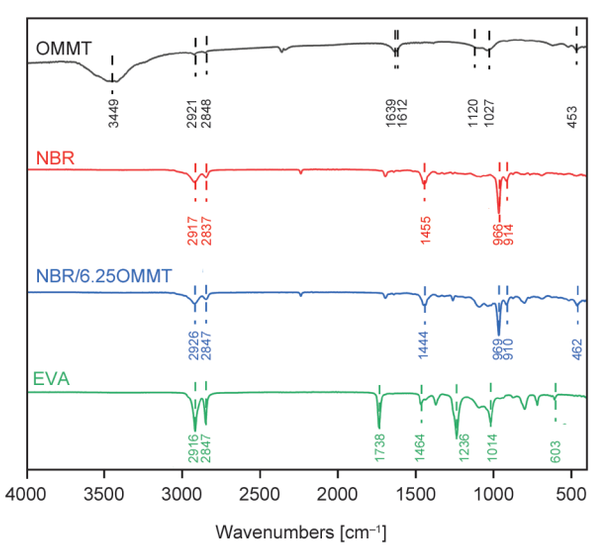

Figure 1. FT-IR spectra of OMMT, EVA and NBR vulcanizates.

at positions and intensities similar to that of NBR vulcanizate; moreover, the bending vibration absorption peak of the Si–O–Si bond appears at 462 cm^{-1}, indicating the presence of OMMT.

In the EVA spectrum, a strong $–CH_3$ stretching vibration peak is observed near 2916 cm^{-1} and characteristic peaks at 2847 and 1464 cm^{-1} confirm the stretching vibration of $–CH_2$. In addition, stretching vibration peaks of C=O and C–O–C are observed near 1738 and 1236 cm^{-1}, respectively. Stretching vibration peaks of C–C and bending vibration peaks of C–H are observed at 1014 and 603 cm^{-1}, respectively, which are in agreement with the chemical structure of EVA. It is worth noting that a weak characteristic peak is observed at 1100 cm^{-1}, which can be attributed to the ester in EVA.

3.2. Mechanical properties of series of EVA/NBR TPV

Table 1 shows the mechanical characteristics of the series EVA/NBR TPV. Here, the M signifies OMMT, the E denotes OMMT which was incorporated into the EVA phase, the N indicates OMMT which was incorporated into the NBR phase while the T represents OMMT which was added directly into the EVA/NBR TPV blend during the dynamic vulcanization process; moreover, the numbers 5, 7, 9 and 11 represent the OMMT dosage compared to that of the EVA/NBR TPV. For instance, 5ME, 5MN and 5MT refer to 5 phr OMMT which was added into the EVA phase, NBR phase and EVA/NBR TPV, respectively. It can be seen from Table 1 that for the TPV specimen where OMMT was incorporated in the NBR pre-blend, the tensile strength, elongation at break, tear strength and hardness of TPV initially increased and then decreased with the increasing OMMT dosage. Notably, the TPV exhibited optimum mechanical properties when the OMMT dosage was 9 phr.

From Table 1, we can also observe the improvement in mechanical properties due to the reinforcing effects of OMMT. The macromolecular chains of NBR are able to intercalate within the OMMT layers, where the OMMT effectively restricts the mobility of the NBR chains. This restriction acts as the physical crosslinking points within the NBR matrix, enhancing the interaction forces within the rubber's crosslink network. Consequently, the mechanical properties of NBR are improved, which enhances the overall mechanical property of the TPV. When the OMMT dosage was increased to 11 phr, the TPV specimen exhibited a significant decline in tensile strength, elongation at break and tear strength. The reduction in mechanical properties is primarily attributed to the self-agglomeration of OMMT at higher concentrations, which would lead to the poor dispersion within the NBR matrix. Furthermore, compared with that of TPV where OMMT was added in EVA and NBR, the tensile strength, tear strength and hardness were the highest where OMMT was added during the dynamic vulcanization of TPV.

3.3. Contact angle and SFE of EVA and a series of NBR

Table 2 shows the contact angle and SFE of EVA and a series of NBR vulcanizates. It can be seen from Table 2 that EVA has the highest contact angle and the lowest SFE. Compared with that of EVA, NBR

Table 2 Contact angle and SFE of EVA and a series of NBR.

Specimen (mass ratio)	Contact angle [°]	SFE [$mN \cdot m^{-1}$]
EVA	100.4±0.9	16.92±1.0
NBR	98.4±1.1	17.96±1.3
NBR/6.25OMMT	95.3±1.5	18.61±1.8
NBR/8.75OMMT	90.1±1.4	19.90±1.6
NBR/11.25OMMT	88.9±1.3	19.92±1.9
NBR/13.75OMMT	86.1±1.6	19.44±1.5

Table 1. Mechanical properties of series of EVA/NBR TPV.

EVA/NBR/OMMT (mass ratio)	Tensile strength [MPa]	Elongation at break [%]	Tear strength [$kN \cdot m^{-1}$]	Shore A hardness
20/80/0	2.39	571.9	16.50	39
20/80/5ME	2.84	334.3	21.59	47
20/80/5MT	3.37	383.2	22.85	52
20/80/5MN	2.24	541.5	17.97	45
20/80/7MN	2.83	571.2	20.58	46
20/80/9MN	2.91	584.9	21.54	50
20/80/11MN	2.68	555.5	17.95	50

has a lower contact angle and a higher SFE, indicating that it is more hydrophilic than that of EVA. Increasing OMMT powder content in NBR, the contact angle of NBR/OMMT gradually decreases and the SFE gradually increases, demonstrating the enhancement of NBR's hydrophilicity by OMMT.

3.4. Hydrophilicity behavior of the EVA/NBR TPV surfaces molded with paper sheet

Figure 2 illustrates the contact angle and SFE for EVA/NBR TPV surfaces (mass ratio 20/80) molded with the series paper sheets. From Figure 2a, it can be found that the contact angle between the untreated TPV surface and the deionized water changes over time. The initial contact angle when the droplet's point of contacts with the TPV surface is approximately 102.8°; subsequently, the contact angle decreases to around 77.2°, followed by a stable period. However, for the TPV surface molded with No. 400 paper sheets, the initial contact angle is approximately 100.2° and there is a rapid and continuous decrease in the contact angle; moreover, the contact angle is 0.3° at 47.4 s, indicating the superwettability behavior. The similar superwettability phenomenon could also be observed on TPV surfaces molded with No. 1000 and No. 1500 paper sheets, where the water droplets could ultimately spread, confirming the remarkable superwettability behavior. Comparing with the superhydrophilic behavior of the TPV surfaces molded with the series paper sheets, it is obvious that the TPV surface molded with No. 1000 paper sheets could achieve the final contact angle of 0.2° within 16.0 s, which was much shorter than that of the No. 400 (47.4 s) and No. 1500 (43.5 s) sandpaper-molded surfaces. The surface molded with No. 1000 paper sheets demonstrates the pronounced superwettability behavior. The distinct shapes of the three curves in Figure 2a could be attributed to variations in the uniformity of the TPV surface at the points of contact with the droplets. The heterogeneity in the micro region induces the water droplet movement, imparting the dynamic ultra-wettability to the molded TPV surface and exhibiting the Marangoni effect of droplet movement [43, 44]. Different locations on the surface may have different surface tension differences, leading to inconsistent changes in the contact angle [6]. Compared to the surfaces of TPV molded with No. 400 and No. 1500 paper sheets, the surface molded with No. 1000 sandpaper may exhibit the greater uniformity. Consequently, droplets are more likely to initially contact areas of the surface where the difference in surface tension is most pronounced, thereby enhancing the superhydrophilic effect observed [17, 45].

Figure 2b shows the SFE of EVA/NBR TPV surfaces (mass ratio 20/80) molded with the series paper sheets. It is evident that the SFE of the series TPV surfaces prepared in this experiment is higher compared to the SFE of traditional non-polar polymer surfaces, while the SFE values are close to 30.0 $mN \cdot m^{-1}$. Compared with the specimens in Figure 2b, the SFE of the surface molded with No. 1000 paper sheets is relatively high (29.1 $mN \cdot m^{-1}$), indicating the good superhydrophilic property.

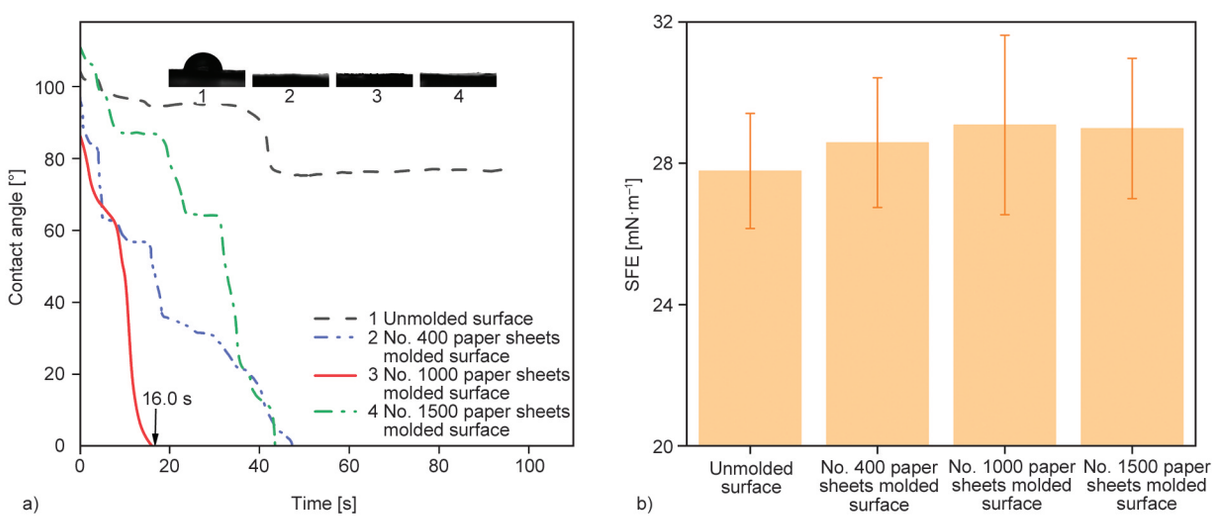

Figure 2. Hydrophilicity behavior of the series EVA/NBR TPV (mass ratio 20/80) surfaces molded with No. 400, No. 1000 and No. 1500 paper sheets and the unmolded TPV surface a) variation of contact angle over time; b) SFE of TPV surfaces.

Figure 3 shows the FE-SEM image of the series EVA/NBR TPV (mass ratio 20/80) surfaces molded with the series paper sheets. As shown in Figure 3a, the unmolded TPV surface is not smooth and only exhibits the slight roughness, and water droplets cannot spread completely on the surface. Figure 3b shows the surface morphology molded by No. 400 paper sheet where the incomplete tearing strips results in the scattered rough structure. Usually, the tearing strips are mainly formed by the EVA matrix, leading to the heterogeneous surface. The unique heterogeneous microstructure and the difference in the surface polarity between NBR and EVA lead to the SFE gradient in the micro-region. Along the horizontally interface, water in the region with the low SFE will move to the area with the high SFE under the driving force brought by the SFE difference in the micro-region. When the water droplets contacted with the molded TPV surface, water droplets preferentially expand to the NBR phase due to its rich polarity and the higher SFE. Accompanied by the continuous movement of water droplets, they will eventually completely diffuse in the molded TPV surface. The unique microstructure reduces the hydrophobicity of the TPV surface, potentially explaining why the water droplets can effectively diffuse in the molded TPV surface. Figure 3c depicts the surface molded by No. 1000 paper sheets, showing a similar microstructure to that of the No. 400 while with a more precise roughness and evident tearing strips, which enhances the phase separation between the rubber and the thermoplastic, creating a more noticeable SFE gradient. This also contributes to the increased hydrophilicity compared to that of the No. 400 paper sheets. Figure 3d shows the EVA/NBR TPV surface molded by No. 1500, exhibiting a similar microstructure to that molded by No. 400 and No. 1000 paper sheets.

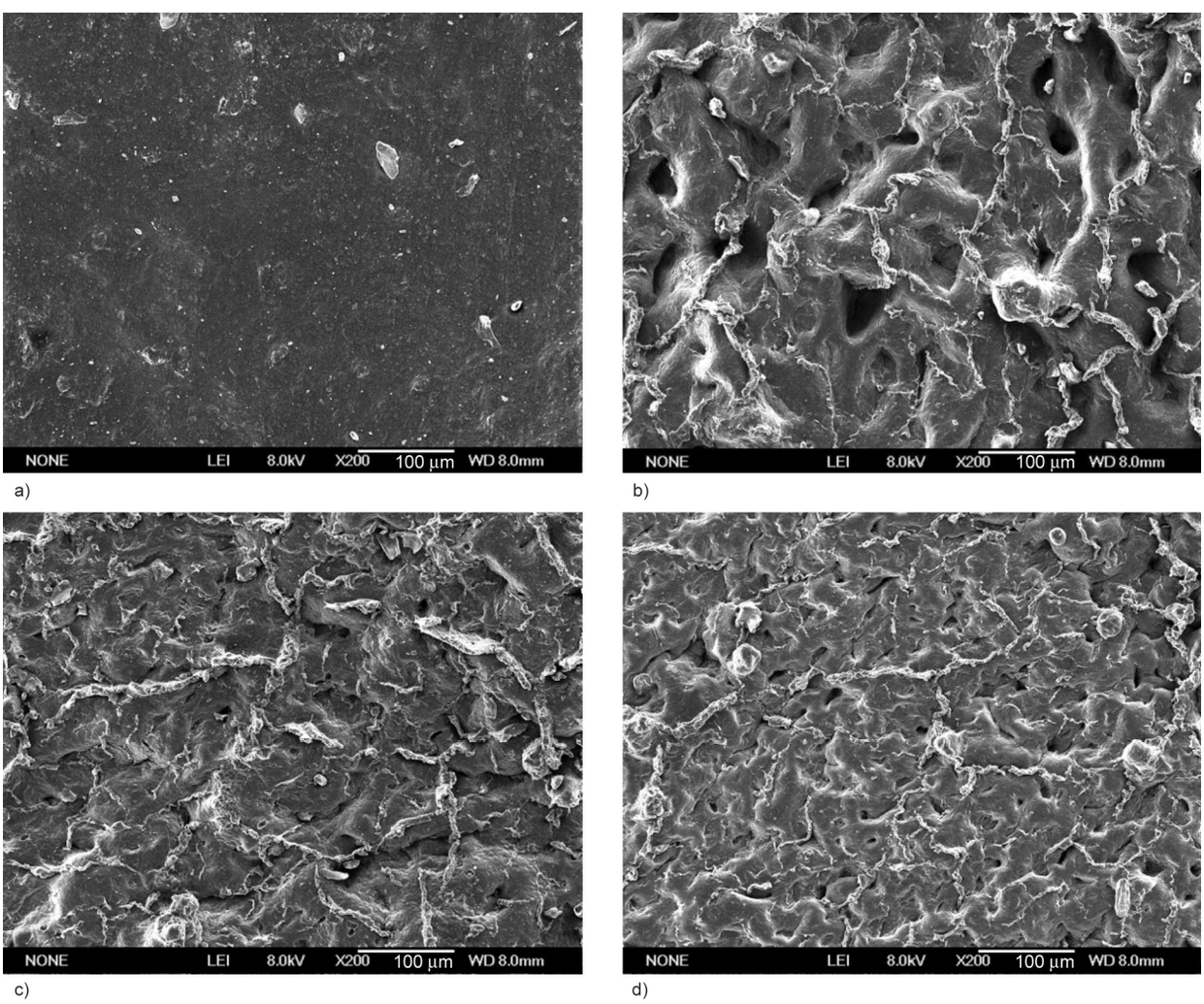

Figure 3. FE-SEM images of the series EVA/NBR TPV (mass ratio 20/80) surfaces: a) unmolded; b) molded with No. 400 paper sheet; c) molded with No. 1000 paper sheet; d) molded with No. 1500 paper sheet.

3.5. Hydrophilicity behavior of the EVA/NBR/OMMT TPV surface

Figure 4 illustrates the influence time on the contact angle and the SFE of the series OMMT-modified EVA/NBR TPV surfaces molded with the No. 1000 paper sheet. Figure 4a shows the influence of incorporation method of OMMT in EVA/NBR on the contact angel of the molded TPV surface. Surprisingly, the introduction of OMMT in the rubber phase of TPV demonstrates a significant enhancement in the superhydrophilic property. It is observed that the intial contact angle of the molded TPV surface where OMMT powder was incorporated into the NBR preblend is lower than that of the molded TPV surface where the OMMT powder was incorporated into the EVA matrix and the TPV blend. The difference is attributed to the polarity difference between the NBR phase and the EVA phase in the prepared TPV blends. The cyano group in the NBR phase exhibits the strong polarity, while the vinyl acetate (VA) in the EVA phase has the relatively weak polarity. However, the OMMT powder itself possesses the strong polarity. When OMMT was added into the NBR preblend, the polarity of the NBR phase will be increased greatly, leading to the greater polarity difference between the EVA phase and the NBR phase in the TPV. This will inevitably result in the increasing SFE difference and the pronounced Marangoni effect, leading to the increased superhydrophilic behavior and the rapid diffusion of water droplet in the surface of the molded EVA/NBR TPV surface.

Figure 4b shows the influence of the OMMT dosage in the NBR phase of EVA/NBR/MN TPV on the contact angle of the molded surface. The contact angle testing on the series of molded surfaces of EVA/NBR TPV reveal that all surfaces ultimately achieve

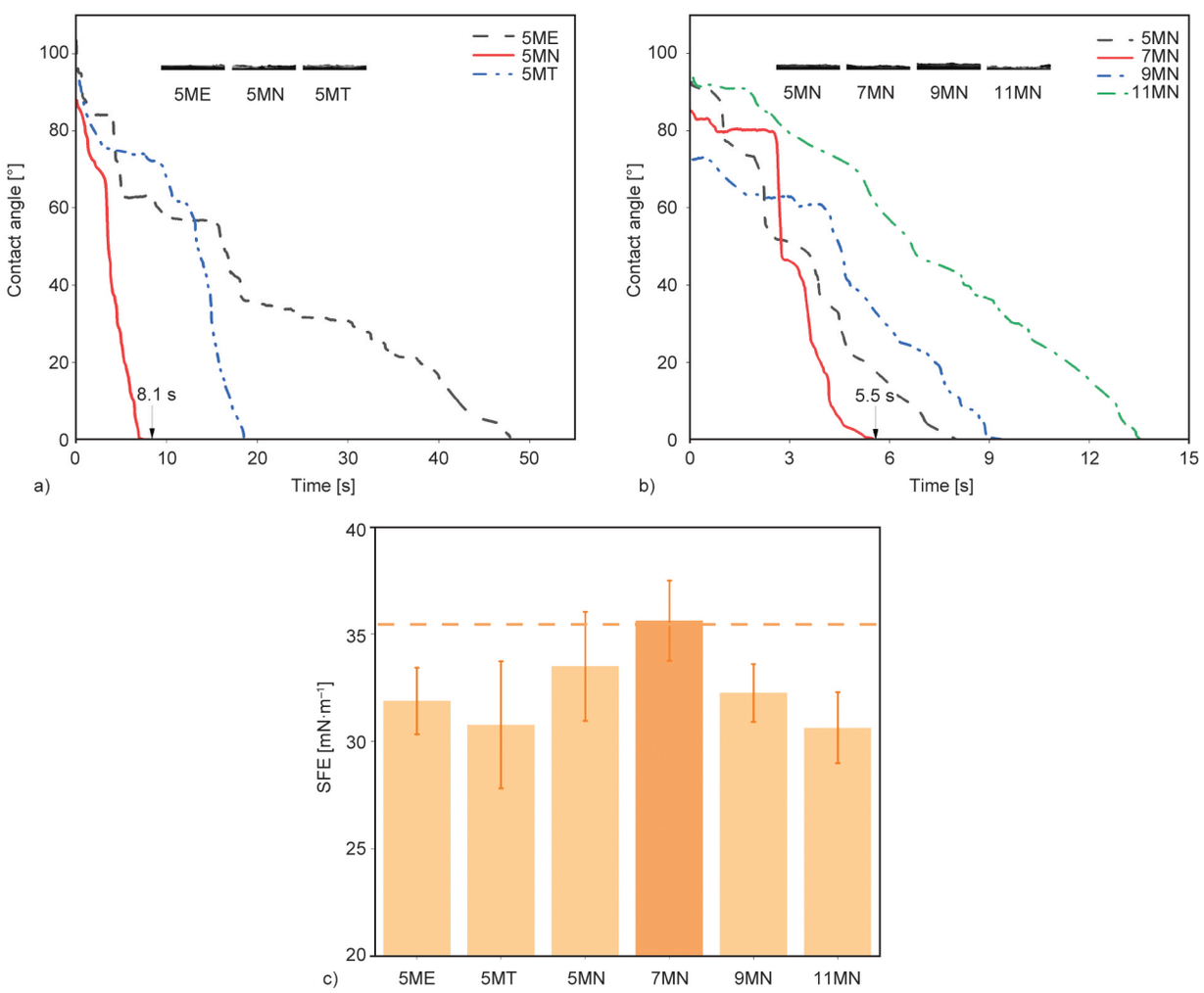

Figure 4. Series EVA/NBR/OMMT TPV (mass ratio 20/80) surfaces molded with No. 1000 paper sheets a) the influence of OMMT incorporation method on the contact angle of the molded TPV surface; b) the influence of OMMT dosage in NBR pre-blend on the contact angle of the molded TPV surface; c) SFE of series EVA/NBR/OMMT TPV molded surfaces.

the superhydrophilicity behavior. Notably, the existence of 7 phr OMMT results in the shortest superhydrophilic response time (5.5 s), compliant with the standard for superhydrophilic surfaces and showing the obvious superhydrophilic behavior. Increasing OMMT dosage in the NBR phase of EVA/NBR/MN TPV, the polarity difference between the EVA and NBR phases is increased, amplifying the Marangoni effect and thereby enhancing the superhydrophilic response rate. The research results of Chandran and coworker [46, 47] indicate that the inorganic powder is more prone to migrate into the plastic phase with higher fluidity. Increasing the OMMT dosage, the OMMT particles will be likely to migrate to the interface of the EVA/NBR dual phases due to the high fluidity of EVA melt. The migration will reduce the polarity difference between the EVA and NBR phase, resulting in the decreasing rate of superhydrophilic response. The variations in the shapes of the four curves in Figure 4b, similar to those observed in Figure 2b, may be attributed to differences in surface tension across various parts of the surface.

Figure 4c presents the SFE data of the prepared EVA/ NBR TPV surface molded with No. 1000 paper sheets where the OMMT dosages and incorporation method were different. It can be seen that form Figure 4c that the SFE of the EVA/NBR TPV specimen where 7 phr OMMT was incorporated in the NBR pre-blend is the highest (35.6 $mN \cdot m^{-1}$), which is relatively closed to the surface tension of water (75.8 $mN \cdot m^{-1}$).

Figure 5 shows the FE-SEM images of the molded and unmolded TPV surfaces with different OMMT incorporation method and OMMT dosage. It is believed that the distinctive two-phase microstructure in TPV induces a difference in surface tension between the EVA and NBR phases, contributing to the obvious hydrophilic behavior. As can be seen from the Figure 5a–5c, we can find the tearing strips in the 5ME and 5MT specimen surface; however, the tearing strips in the 5MN specimen surface is denser and significantly than that in the 5ME and 5MT molded surfaces. The dense tearing strips play a significant role in the superhydrophilic behavior in the EVA/NBR TPV surface. The increasing tearing strips directly correlates with a conspicuous separation phenomenon between the NBR and EVA interface, enhancing the diffusion rate of water droplets in the molded TPV surface and the Marangoni effect. Figure 5d–5f shows the SEM images of the unmolded surfaces of 5ME, 5MN and 5MT. It is obvious that all the surfaces exhibit the relatively flat surface, distinguishing them from the SEM images of that of the molded TPV surfaces.

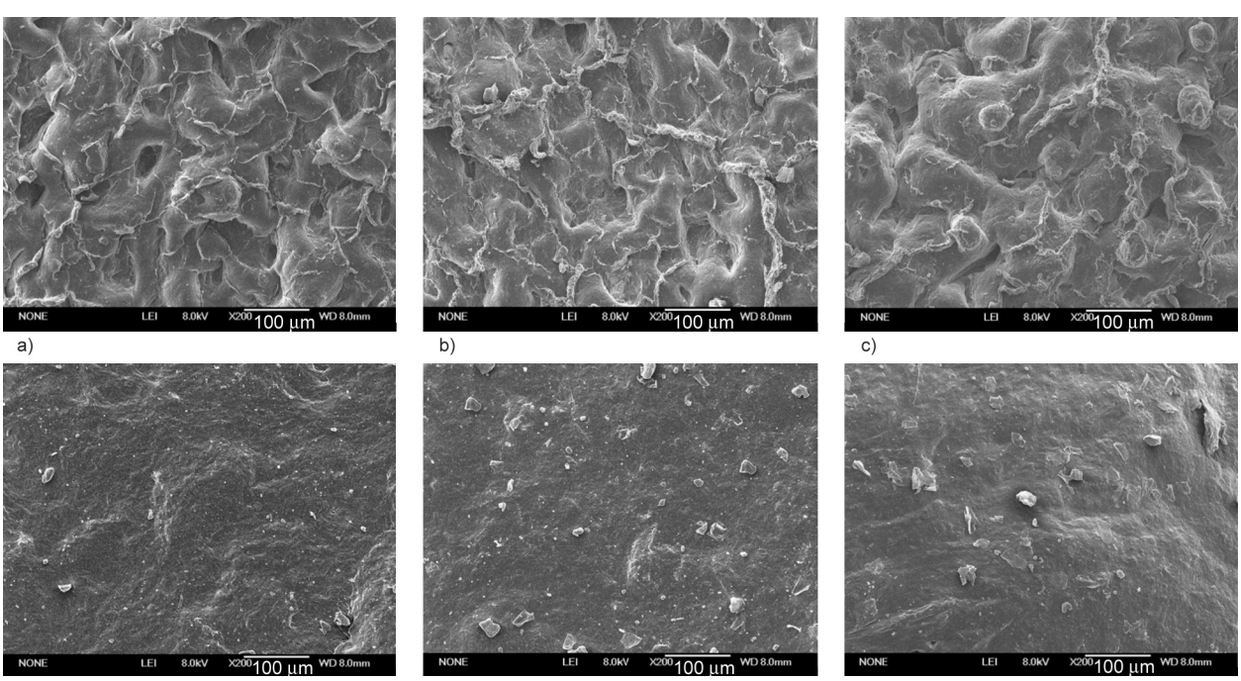

Figure 5. FE-SEM of series EVA/NBR/OMMT TPV (mass ratio 20/80) surface a) 5ME surface molded with No. 1000 paper sheet; b) 5MN surface molded with No. 1000 paper sheet; c) 5MT surface molded with No. 1000 paper sheet; d) 5ME unmolded surface; e) 5MN unmolded surface; f) 5MT unmolded surface.

3.6. Critical pressure test for different liquid

Figure 6 is a schematic of the device which can be used for P_m testing and oil-water separation. The device enables the continuous oil-water and oil-oil separation through the pressure response of the valve. The oil-water and oil-oil separation method is carried out by the direct suction pressure response oil-water or oil-oil separation device, which differs from the traditional gravity-driven process and offers the high separation efficiency [48].

Table 3 shows the P_m data of several liquids where the suction force can exactly provide the driving force for the liquid to pass through the gap of the winded EVA/NBR/7MN TPV (mass ratio 20/80/7) film. The superhydrophilic EVA/NBR TPV film prepared exhibits the significantly different Pm for water and different oils, indicating its potential for use in oil-water separation applications.

3.7. Self-cleaning behavior of the EVA/NBR/OMMT TPV surface

During the oil-water separation process and in daily application, granular pollutants such as oil residue and dust often remain in the surface of the TPV film. This would decrease the superhydrophilicity and reduce the efficiency of oil-oil separation. In the daily life, the superhydrophilic surface can exhibit the ability to clear the accumulated pollutants when exposed to water and oil droplets environment, maintaining the dust-free state and showing the material's self-cleaning characteristics. In order to confirm the self-cleaning behavior of the prepared superhydrophilic EVA/NBR TPV film, dust was used as a pollutant material, and the self-cleaning behavior of the film's surface was assessed using air, water and oil (dodecane). Figure 7 reflects the self-cleaning behavior of the superhydrophilic TPV surface. It can be seen that the wind sweeping, water and oil (dodecane) droplets can enhance the self-cleaning behavior of the superhydrophilic surface, effectively solving the potential pollution issues in both daily life and industrial applications.

3.8. Durability of the EVA/NBR/OMMT TPV surface

Although the great progress has been achieved in the development and preparation of superhydrophilic materials, there are still some key problems and challenges in the basic research and the industrial application. One of the major issues is the durability of the superhydrophilic materials. Most literature reports indicated the relatively short experimental periods and there is a significant gap in the industrial use cycle. Excessive sample storage time may cause the material to separate from the matrix surface or alter the surface microstructure, leading to the loss of its superhydrophilic properties. In order to assess

Table 3. P_m data of several liquids where the suction force can provide the driving force for the liquid to pass through the gap of the winded EVA/NBR/7MN TPV (mass ratio 20/80/7) film molded with No. 1000 paper sheets (film gap 50 μm).

Type of the liquids	*Pm* [kPa]
Water	2.65
Cyclohexane	1.85
Dodecane	0.90
Ethylene glycol	6.35

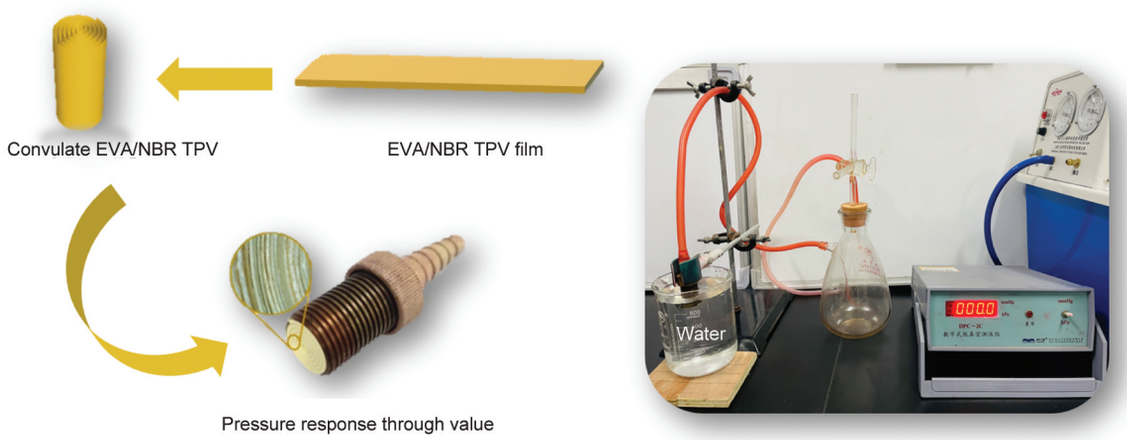

Figure 6. Schematic diagram of critical pressure testing and continuous oil-water separation device through the direct suction pressure response oil-water separation valve.

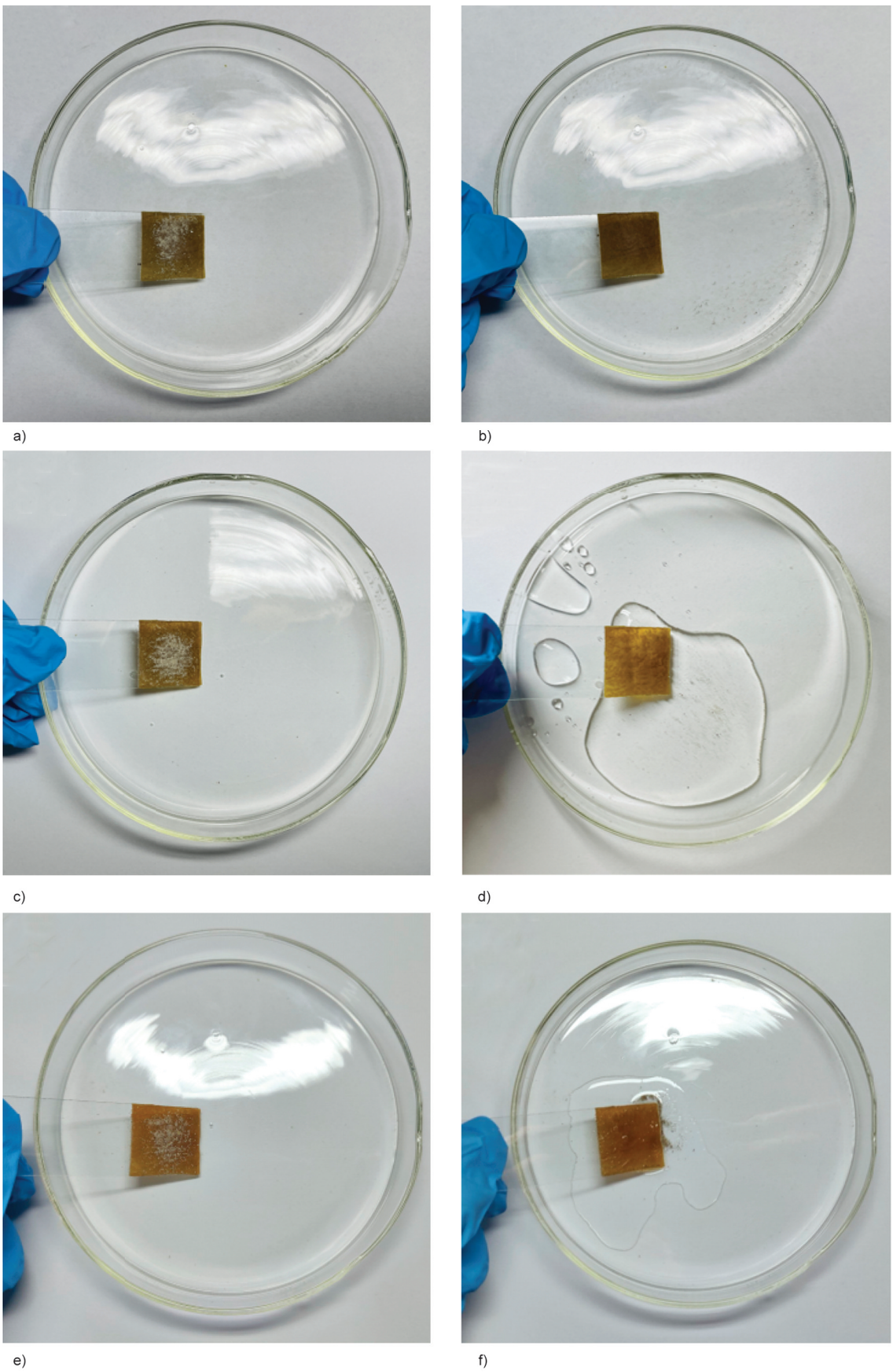

Figure 7. Self-cleaning behavior of EVA/NBR/7MN TPV (mass ratio 20/80/7) superhydrophilic surface molded with No. 1000 paper sheets a), c), e) surface with dust; b) cleaning surface using air; d) cleaning surface using water; f) cleaning surface using oil (dodecane).

the durability of the surface of the prepared superhydrophilic EVA/NBR TPV film, durability testing was conducted.

Figure 8 shows the influence of placement time on the contact angle of the superhydrophilic EVA/NBR TPV surface. Notably, even after 30 days of placement, the time required for the contact angle to reach 0.0° remains virtually unchanged. Furthermore, the contact angle for the TPV film placed for 60 days can still reach 0.0° with a slight increase in response time. The test demonstrated that the superhydrophilic EVA/NBR TPV film has the excellent stability and durability, and its superhydrophilic behavior can remain even over a longer period of time.

4. Conclusions

In this research, a simple templating method was used for the first time to construct the superhydrophilic surface of EVA/NBR TPV by molding with No. 1000 paper sheets and the rate of superhydrophilic response was further optimized with the introduction of OMMT. Experimental evidence has shown that the EVA/NBR TPV surface molded with No. 1000 paper sheets exhibited the fastest superhydrophilic response rate. The mechanism of the superhydrophilic surface of EVA/NBR TPV was proposed, which is attributed to the Marangoni effect. OMMT powder was incorporated into the EVA phase, NBR phase and EVA/NBR TPV, respectively. The results confirmed that the EVA/NBR/MN TPV surface displayed the fast superhydrophilic response time, affirming the involvement of the Marangoni effect. Surprisingly, the superhydrophilic response time of the EVA/NBR/7MN TPV molded surface was significantly improved by incorporation of 7 phr OMMT in the NBR phase, reaching an angle of approximately 0.0° within 5.5 s. The results of self-cleaning behavior, critical pressure test and durability testing indicated that EVA/NBR/7MN TPV surface molded with the No. 1000 paper sheets has the excellent self-cleaning property and the outstanding durability. Moreover, the significant difference in the Pm of different liquids indicate its potential application prospects in oil-water and oil-oil separation. The experimental results have expanded the preparation methods and application scenarios of superhydrophilic surfaces based on polymers. Compared with the other superhydrophilic polymer materials, the prepared superhydrophilic EVA/NBR/7MN TPV film has the advantages of low cost, simple preparation method and good durability, which is beneficial for large-scale applications in production and daily life [34–37].

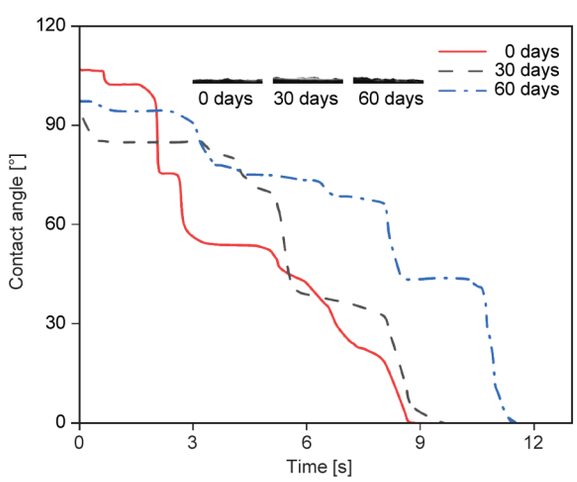

Figure 8. Influence of placement time on the contact angle of EVA/NBR/7MN TPV surface (mass ratio 20/80/7) molded with No. 1000 paper sheets.

Acknowledgements

The work was supported by the Shandong Provincial Natural Science Foundation, China (ZR2021ME028).

References

[1] Liu F. F., Sun Y. T., Wang Z. B.: Facile design of heat-triggered shape-memory ethylene-acrylic acid copolymer/chloroprene rubber thermoplastic vulcanizates. Express Polymer Letters, **14**, 281–293 (2020). https://doi.org/10.3144/expresspolymlett.2020.24

[2] Soares B. G., Santos D. M., Sirqueira A. S.: A novel thermoplastic elastomer based on dynamically vulcanized polypropylene/acrylic rubber blends. Express Polymer Letters, **2**, 602–613 (2008). https://doi.org/10.3144/expresspolymlett.2008.72

[3] Magioli M., Sirqueira A. S., Soares B. G.: The effect of dynamic vulcanization on the mechanical, dynamic mechanical and fatigue properties of TPV based on polypropylene and ground tire rubber. Polymer Testing, **29**, 840–848 (2010). https://doi.org/10.1016/j.polymertesting.2010.07.008

[4] Si Y., Dong Z., Jiang L.: Bioinspired designs of superhydrophobic and superhydrophilic materials. ACS Central Science, **4**, 1102–1112 (2018). https://doi.org/10.1021/acscentsci.8b00504

[5] Dey A., Chandrabose G., Ghosh P., Damptey L. A., Clark A. H., Selvaraj V., Kumar R. V., Braithwaite N. S. J., Zhuk S., Dalapati G. K., Ramakrishna S., Krishnamurthy S.: Atmospheric pressure plasma engineered superhydrophilic CuO surfaces with enhanced catalytic activities. Applied Surface Science, **564**, 150413 (2021). https://doi.org/10.1016/j.apsusc.2021.150413

[6] Aydemir C., Altay B. N., Akyol M.: Surface analysis of polymer films for wettability and ink adhesion. Color Research and Application, **46**, 489–499 (2021). https://doi.org/10.1002/col.22579

[7] Darmanin T., Guittard F.: Wettability of conducting polymers: From superhydrophilicity to superoleophobicity. Progress in Polymer Science, **39**, 656–682 (2014). https://doi.org/10.1016/j.progpolymsci.2013.10.003

[8] Rasitha T. P., Thinaharan C., Vanithakumari S. C., Philip J.: A simple approach for fabrication of superhydrophobic titanium surface with self-cleaning and bouncing properties. Colloids and Surfaces A: Physicochemical and Engineering Aspects, **636**, 128110 (2022). https://doi.org/10.1016/j.colsurfa.2021.128110

[9] Ma T., Ma J., Yang C., Zhang J., Cheng J.: Robust, multiresponsive, superhydrophobic, and oleophobic nanocomposites *via* a highly efficient multifluorination strategy. ACS Applied Materials and Interfaces, **13**, 28949–28961 (2021). https://doi.org/10.1021/acsami.1c07048

[10] Zhang Y., Wang T., Lv Y.: Durable biomimetic two-tier structured superhydrophobic surface with ultralow adhesion and effective antipollution property. Langmuir, **39**, 2548–2557 (2023). https://doi.org/10.1021/acs.langmuir.2c02756

[11] Guan H., Li R., Lian R., Cui J., Ou M., Liu L., Chen X., Jiao C., Kuang S.: A biomimetic design for efficient petrochemical spill disposal: CoFe-PBA modified superhydrophobic melamine sponge with mechanical/chemical durability and low fire risk. Journal of Hazardous Materials, **459**, 132041 (2023). https://doi.org/10.1016/j.jhazmat.2023.132041

[12] Peng J., Wu L., Zhang H., Wang B., Si Y., Jin S., Zhu H.: Research progress on eco-friendly superhydrophobic materials in environment, energy and biology. Chemical Communications, **58**, 11201–11219 (2022). https://doi.org/10.1039/D2CC03899D

[13] Açık G.: Synthesis, properties and enzymatic biodegradation behavior of fluorinated poly(ε-caprolactone)s. Express Polymer Letters, **14**, 272–280 (2020). https://doi.org/10.3144/expresspolymlett.2020.23

[14] Bai L., Wang X., Guo X., Liu F., Sun H., Wang H., Li J.: Superhydrophobic electrospun carbon nanofiber membrane decorated by surfactant-assisted *in-situ* growth of ZnO for oil–water separation. Applied Surface Science, **622**, 156938 (2023). https://doi.org/10.1016/j.apsusc.2023.156938

[15] Saji V. S.: Superhydrophobic surfaces and coatings by electrochemical methods – A review. Journal of Adhesion Science and Technology, **37**, 137–161 (2023). https://doi.org/10.1080/01694243.2022.2031462

[16] Sethi S. K., Kadian S., Gogoi R., Manik G.: Layer-by-layer fabrication of self-cleaning superhydrophobic surface made from carboxymethylcellulose and ZnO quantum dots: A combined experimental and computational study. Surfaces and Interfaces, **37**, 102752 (2023). https://doi.org/10.1016/j.surfin.2023.102752

[17] Drelich J., Chibowski E., Meng D. D., Terpilowski K.: Hydrophilic and superhydrophilic surfaces and materials. Soft Matter, **7**, 9804–9828 (2011). https://doi.org/10.1039/C1SM05849E

[18] Wang R., Hashimoto K., Fujishima A., Chikuni M., Kojima E., Kitamura A., Shimohigoshi M., Watanabe T.: Light-induced amphiphilic surfaces. Nature, **388**, 431–432 (1997). https://doi.org/10.1038/41233

[19] Syafiq A., Vengadaesvaran B., Pandey A. K., Rahim N. A.: Superhydrophilic smart coating for self-cleaning application on glass substrate. Journal of Nanomaterials, **2018**, 6412601 (2018). https://doi.org/10.1155/2018/6412601

[20] Lai Y., Tang Y., Gong J., Gong D., Chi L., Lin C., Chen Z.: Transparent superhydrophobic/superhydrophilic TiO_2-based coatings for self-cleaning and anti-fogging. Journal of Materials Chemistry, **22**, 7420–7426 (2012). https://doi.org/10.1039/C2JM16298A

[21] Zhu Y., Tso C. Y., Ho T. C., Leung M. K., Yao S., Qiu H.: Heat transfer enhancement on tube surfaces with biphilic nanomorphology. Applied Thermal Engineering, **180**, 115778 (2020). https://doi.org/10.1016/j.applthermaleng.2020.115778

[22] Li S., Huang L., Wang D., Zhou S., Sun X., Zhao R., Wang G., Yao T., Zhao K., Chen R.: A review of 3D superhydrophilic porous materials for oil/water separation. Separation and Purification Technology, **326**, 124847 (2023). https://doi.org/10.1016/j.seppur.2023.124847

[23] Rasouli S., Rezaei N., Hamedi H., Zendehboudi S., Duan X.: Superhydrophobic and superoleophilic membranes for oil-water separation application: A comprehensive review. Materials and Design, **204**, 109599 (2021). https://doi.org/10.1016/j.matdes.2021.109599

[24] Kaya A. S. T., Cengiz U.: Fabrication and application of superhydrophilic antifog surface by sol-gel method. Progress in Organic Coatings, **126**, 75–82 (2019). https://doi.org/10.1016/j.porgcoat.2018.10.021

[25] Thi Q. H., Man P., Huang L., Chen X., Zhao J., Ly T. H.: Superhydrophilic 2D carbon nitrides prepared by direct chemical vapor deposition. Small Science, **3**, 2200099 (2023). https://doi.org/10.1002/smsc.202200099

[26] Sun J., Li Y., Liu G., Chu F., Chen C., Zhang Y., Tian H., Song Y.: Patterning a superhydrophobic area on a facile fabricated superhydrophilic layer based on an inkjet-printed water-soluble polymer template. Langmuir, **36**, 9952–9959 (2020). https://doi.org/10.1021/acs.langmuir.0c01769

[27] Huang W., Deng W., Lei M., Huang H.: Superhydrophilic porous TiO_2 film prepared by phase separation through two stabilizers. Applied Surface Science, **257**, 4774–4780 (2011). https://doi.org/10.1016/j.apsusc.2010.11.125

[28] Liao K-S., Wan A., Batteas J. D., Bergbreiter D. E.: Superhydrophobic surfaces formed using layer-by-layer self-assembly with aminated multiwall carbon nanotubes. Langmuir, **24**, 4245–4253 (2008). https://doi.org/10.1021/la703730b

[29] Zhang L., Zhao N., Xu J.: Fabrication and application of superhydrophilic surfaces: A review. Journal of Adhesion Science and Technology, **28**, 769–790 (2014). https://doi.org/10.1080/01694243.2012.697714

[30] Tettey K. E., Dafinone M. I., Lee D.: Progress in superhydrophilic surface development. Materials Express, **1**, 89–104 (2011). https://doi.org/10.1166/mex.2011.1021

[31] Mozetič M.: Plasma-stimulated super-hydrophilic surface finish of polymers. Polymers, **12**, 2498 (2020). https://doi.org/10.3390/polym12112498

[32] Hosseini M. S., Sadeghi M. T., Khazaei M.: Wettability alteration from superhydrophobic to superhydrophilic *via* synthesized stable nano-coating. Surface and Coatings Technology, **326**, 79–86 (2017). https://doi.org/10.1016/j.surfcoat.2017.07.032

[33] Ma Z., Liang S., Xiao K., Wang X., Li M., Huang X.: Superhydrophilic polyvinylidene fluoride membrane with hierarchical surface structures fabricated *via* nanoimprint and nanoparticle grafting. Journal of Film Science, **612**, 118332 (2020). https://doi.org/10.1016/j.memsci.2020.118332

[34] Tsougeni K., Vourdas N., Tserepi A., Gogolides E., Cardinaud C.: Mechanisms of oxygen plasma nanotexturing of organic polymer surfaces: From stable super hydrophilic to super hydrophobic surfaces. Langmuir, **25**, 11748–11759 (2009). https://doi.org/10.1021/la901072z

[35] Zheng J., Feng J., Zhong M.: Fabricating polymer superhydrophilic/superhydrophobic surfaces by replica\ molding method using $CaCO_3$ particles as template (in Chinese). Acta Polymerica Sinica, **10**, 1186–1192 (2010). https://doi.org/10.3724/SP.J.1105.2010.09377

[36] Usha Z. R., Babiker D. M. D., Yu R., Yang J., Chen W., Chen X., Li L.: Super hydrophilic modified biaxially oriented polypropylene microporous membrane for excellent gravity-driven oil/water emulsion separation. Journal of Membrane Science, **660**, 120840 (2022). https://doi.org/10.1016/j.memsci.2022.120840

[37] Chen N., Chen S., Yin H., Zhu B., Liu M., Yang Y., Zhang Z., Wei G.: Durable underwater super-oleophobic/super-hydrophilic conductive polymer membrane for oil-water separation. Water Research, **243**, 120333 (2023). https://doi.org/10.1016/j.watres.2023.120333

[38] Salyer I. O., Kenyon A. S.: Structure and property relationships in ethylene-vinyl acetate copolymers. Journal of Polymer Science Part A-1: Polymer Chemistry, **9**, 3083–3103 (1971). https://doi.org/10.1002/pol.1971.150091101

[39] Kojima T., Yanagisawa T.: The evaluation of accelerated test for degradation a stacked a-Si solar cell and EVA films. Solar Energy Materials and Solar Cells, **81**, 119–123 (2004). https://doi.org/10.1016/j.solmat.2003.09.003

[40] Liu J., Li X., Xu L., Zhang P.: Investigation of aging behavior and mechanism of nitrile-butadiene rubber (NBR) in the accelerated thermal aging environment. Polymer Testing, **54**, 59–66 (2016). https://doi.org/10.1016/j.polymertesting.2016.06.010

[41] Sreenivasan D. P., Sujith A., Rajesh C.: Cure, mechanical and swelling properties of biocomposites from chicken feather fibre and acrylonitrile butadiene rubber. Journal of Polymers and the Environment, **26**, 2720–2729 (2018). https://doi.org/10.1007/s10924-017-1165-4

[42] Zhang X., Feng R., Wang J., Wang W., Hua J., Wang Z.: Pressure response through valve for continuous oil-water separation based on a flexible superhydrophobic/superoleophilic thermoplastic vulcanizate film. Macromolecular Materials and Engineering, **306**, 2000745 (2021). https://doi.org/10.1002/mame.202000745

[43] Nikolov A. D., Wasan D. T., Chengara A., Koczo K., Policello G. A., Kolossvary I.: Superspreading driven by Marangoni flow. Advances in Colloid and Interface Science, **96**, 325–338 (2002). https://doi.org/10.1016/S0001-8686(01)00087-2

[44] Xu X., Luo J.: Marangoni flow in an evaporating water droplet. Applied Physics Letters, **91**, 124102 (2007). https://doi.org/10.1063/1.2789402

[45] Pasias D., Koutsokeras L., Passos A., Constantinides G., Balabani S., Kaliviotis E.: Effects of biomechanical properties of blood on surface tension-driven flows in superhydrophilic channels. Physics of Fluids, **34**, 051907 (2022). https://doi.org/10.1063/5.0088643

[46] Shan X., Huang P., Yang L. J., Feng R. T., Wang Z. B.: Robust polypropylene/ethylene-propylene-diene terpolymer thermoplastic vulcanizates film for green oil–water separation. Journal of Polymer Research, **29**, 94 (2022). https://doi.org/10.1007/s10965-022-02948-0

[47] Chandran N., Chandran S., Maria H. J., Thomas S.: Compatibilizing action and localization of clay in a polypropylene/natural rubber (PP/NR) blend. RSC Advances, **5**, 86265 (2015). https://doi.org/10.1039/C5RA14352G

[48] Chandran N., Sarathchandran C., Jose S., Thankappan S., Thomas S.: Organic modifier induced interfacial transformation, morphology and physico-mechanical properties of PP/NR based blend nanocomposites. Composites Part B Engineering, **194**, 108045 (2020). https://doi.org/10.1016/j.compositesb.2020.108045